Russian Geology and Geophysics © 2019, V.S. Sobolev IGM, Siberian Branch of the RAS
Vol. 60, No. 2, pp. 204–214, 2019 *DOI:10.15372/RGG2019016* *Geologiya i Geofizika*

Radon and Tectonic Activities of Crustal Faults: the Case of Central Mongolia

K.Zh. Seminsky [a, ✉], A.A. Bobrov [a], S. Demberel [b]

[a] *Institute of the Earth's Crust, Siberian Branch of the Russian Academy of Sciences, Irkutsk, ul. Lermontova 128, 664033, Russia*
[b] *Institute of Astronomy and Geophysics, Mongolian Academy of Sciences, Ulaanbaatar, 210351, Mongolia*

Received 27 September 2017; received in revised form 5 December 2017; accepted 18 December 2018

Abstract—Examples of two geodynamically active regions in Central Mongolia are used to demonstrate the radon and tectonic activities of faults and find out how their individual parameters affect the radon field. In general, the radon activity of faults increases with the higher contribution of extension in dynamic faulting conditions, with stronger seismic activity, and also in concentrated disjunctive structures at their late evolution stages compared to wide rupture zones at the initial formation stages of their internal structure. Nonuniform structure is an intrinsic property of near-fault radon anomalies, which is defined primarily by nonuniform disruptions of the substrate in the fault zone by ruptures and by spatial variations in the displacement amplitude. Taking the established regularities into account will facilitate a higher efficiency of emanation surveys in studies of seismic hazard associated with crustal faults.

Keywords: faults, soil radon, tectonic activity

INTRODUCTION

The relation between radon and tectonic activities of faults is one of the most complex geodynamics problems due to high sensitivity of gas emanations to various types of internal and external effects. At the same time, internal deformation forces are the primary factor in radon field formation in geochemical settings with standard uranium contents in tectonically active regions, since it is these forces that define the stressed state dynamics of the upper crust, which in turn controls the release of radioactive gas into the atmosphere (Toutain and Baubron, 1999; Li et al., 2016; Tansi et al., 2005; Lombardi and Voltattorni, 2010; Papastefanou, 2010; Utkin and Yurkov, 2010; Seminsky and Demberel, 2013; Koike et al., 2014; Zhou et al., 2017; etc.). Considering the practical utility of assessments of tectonic activity and seismic hazards of faults, it is one of the key reasons behind the increasing number of publications on radon activity of ruptures and relations between gas emanations and seismicity in recent years.

The objective of the present paper is to discuss the relationship between radon and tectonic activity of faults using the examples of two regions in Central Mongolia (see the insert in Fig. 1*A*). These are the area affected by the strong Mogod earthquake (M = 7.8; Jan 05, 1967), and the neighborhood of Ulaanbaatar, where almost half the country's population is concentrated and where seismic activity have increased in recent years. In contrast with our previous studies (Seminsky and Demberel, 2013), here we analyze how radon emanations are affected by the main parameters of faults, which represent their tectonic activity directly or indirectly. These include dynamic faulting conditions (compression, shear, etc.), fault rank, the state of the internal structure, and seismic activity acting as the first approximation of present-day fault movement intensity in the absence of data on fault movement velocities for the study areas.

RESEARCH METHODS

Radon activity is considered in the present paper in ten faults (Table 1, Figs. 1*A* and 2*A*), of which five are represented by faults of the Ulaanbaatar region (Skai, Sharai, Avdar, Gunjiin, and Emeelt) and five by rectilinear segments of major disjunctive faults identified as individual structures for research purposes due to differences in strikes and/or dynamic formation conditions. Thus, the latter are represented by segments of the Hustai fault with different orientations in the neighborhood of the Mongolian capital (1, 2, and 3) (Fig. 1*A*) and branches of the seismic rupture formed in 1967 in the Mogod region in the form of meridional strike-slip fault (Mogod) and northwestern striking thrust (Tulet) (Fig. 2*A*).

Dynamic formation conditions of the studied ruptures are presented in Table 1 according to (Bayasgalan and Jackson, 1999; Bano et al., 2017; Seminsky et al., 2017). Fault ranks were estimated based on total extension of topographic

✉ Corresponding author.
E-mail adress: seminsky@crust.irk.ru (K.Zh. Seminsky)

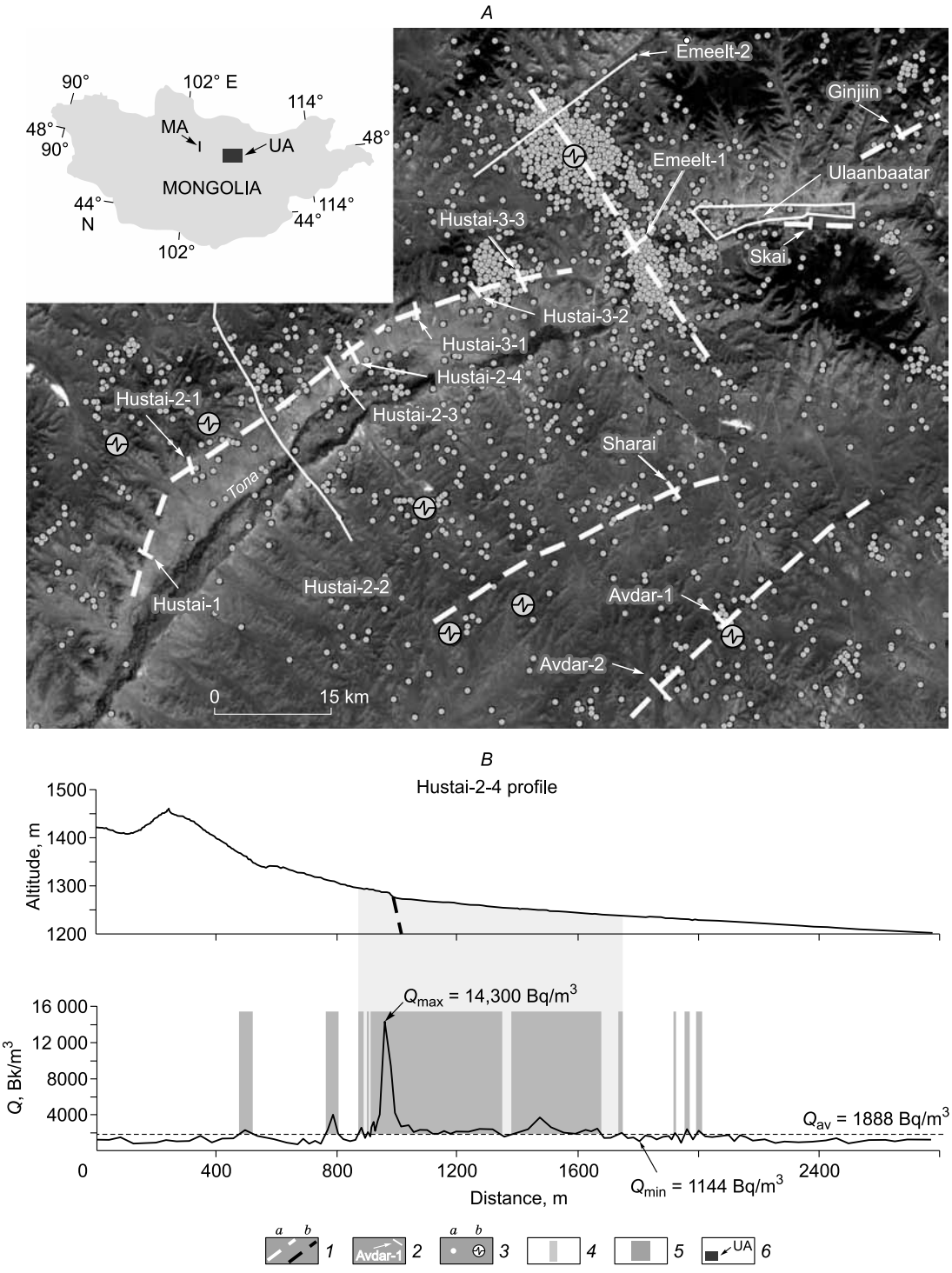

Fig. 1. Locations of the Ulaanbaatar and Mogod study areas in Central Mongolia (insert), layout of emanation survey profiles in the neighborhood of Ulaanbaatar (*A*) and emanation survey results for an individual profile (*B*). A, locations of earthquake epicenters (2000–2014), major faults, and emanation survey profiles in the satellite image of the neighborhood of Ulaanbaatar; *B*, variations in absolute topographic markers (top) and volumetric soil radon activity *Q* (bottom) along the Hustai-2-4 profile intersecting the central segment of the Hustai fault. *1*, faults in the image (*a*) and within the profile (*b*); *2*, emanation profiles and their locations; *3*, earthquake epicenters with magnitudes below (*a*) and above (*b*) three; *4*, near-fault radon anomalies; *5*, profile segments with anomalous soil radon concentrations ($Q > Q_{avg}$); *6*, locations of Mogod (MA) and Ulaanbaatar (UA) emanation survey areas in Central Mongolia. Q_{max} and Q_{min}, radon anomaly parameters used for calculating radon activity (K_Q) for Hustai-2-4 fault.

Table 1. Radon activity parameters of faults in Central Mongolia studied by profile emanation survey

Fault	Fault zone parameters			Name of the radon survey profile	Radon anomaly parameters						
	Rank	Dynamic setting	Seismicity		Year recorded	Q_{avg}, Bq/m^3	Q_{max}, Bq/m^3	Q_{min}, Bq/m^3	K_Q	Radon activity	H, m
2	3	4	5	6	7	8	9	10	11	12	13
Hustai-2	2	Shear with extension	Weak events		**2013, 2014**	**1941**	**9298**	**1368**	**7.3**	**High**	**995**
				Hustai-2-1	2014	1072	2150	762	2.8	Average	350
				Hustai-2-2	2013	2243	6340	1235*	5.1	High	1924
				Hustai-2-3	2013	2560	14,400	1670*	8.6	High	708
				Hustai-2-4	2013	1888	14,300	**1144**	12.5	Ultrahigh	1000
Skai	1	Shear	None		**2012**	**1697**	**6540**	**860***	**7.6**	**High**	**140**
Hustai-3	1	Shear	Weak events		**2014**	**2096**	**4490**	**1429**	**3.3**	**Increased**	**891**
				Hustai-3-1	2014	2871	5040	2060	2.4	Average	1200
				Hustai-3-2	2014	1513	4050	976*	4.1	Increased	636
				Hustai-3-3	2014	1904	4380	1250*	3.5	Increased	837
Sharai	2	Shear	Weak events		**2012**	**1883**	**4040**	**1335***	**3.1**	**Increased**	**660**
Avdar	2	Shear	Weak events		**2011, 2012**	**2124**	**3995**	**1103**	**3.5**	**Increased**	**310**
				Avdar-1	2011	2686	5740	1470	3.9	Increased	300
				Avdar-2	2012	1562	2250	737	3.1	Increased	330
Gunjiin	1	Shear	Weak events		**2011**	**2057**	**6560**	**1371***	**4.8**	**Increased**	80
Emeelt	2	Compression with shear	Weak events		**2014, 2016**	**3516**	**7600**	**2990**	**2.7**	**Average**	1625
				Emeelt-1	2014	2208	6080	1850*	3.3	Increased	650
				Emeelt-2	2016	4824	9120	4130	2.2	Average	2600
Mogod	2	Shear	Strong event of 1967		**2016**	**2801**	**4717**	**1845**	**2.5**	**Average**	537
				Mogod-1	2016	2128	3830	1740	2.2	Average	500
				Mogod-2	2016	4286	7100	2600*	2.7	Average	630
				Mogod-3	2016	1988	3220	1195*	2.7	Average	480
Tulet	1	Compression	Strong event of 1967		**2016**	**1728**	**2525**	**1158**	**2.1**	**Average**	225
				Tulet-1	2016	1742	2430	1100*	2.2	Average	150
				Tulet-2	2016	1714	2620	1216*	2.1	Average	300
Hustai-1	1	Shear	None		**2014**	**1840**	**2730**	**1405***	**1.9**	**Low**	821

Note. Q_{max}, maximum soil radon activity within the near-fault anomaly (anomaly intensity); Q_{min}, minimum soil radon activity beyond the anomaly associated with the fault (*, calculated as an average of estimates in both fault sides); K_Q, radon activity of the fault (anomaly contrast); Q_{avg}, arithmetic mean of Q values measured based on the profile; H, width of the near-fault radon anomaly measured along the profile. Anomaly parameters corresponding to whole faults (or fault segments) are highlighted in bold.

scarps identified in the satellite image (Fig. 1*A*) or soil dislocations formed as a result of fault movements (Fig. 2*A*, *B*). All the studied objects are divided into two groups by their extension, the lengths of second-rank faults (~40 km) being two times the size of first-rank faults (~20 km). Seismic activity of ruptures was estimated qualitatively based on distribution of earthquake epicenters (Fig. 1*A*), which accompanied formation of all the studied objects apart from Skai and Hustai-1 faults, but remained weak (M = 0.5–4.5) in the period of emanation survey. Emeelt fault identified by a wide band (5–10 km) with high epicenter density is seen most clearly in the seismicity. In contrast, the Mogod seismic rupture is associated with a small number of weak earthquakes, which indicates its low present-day activity due to stress relief during the strong event back in 1967.

The research technique was presented in detail earlier (Seminsky and Demberel, 2013) and may be briefly described as follows. To determine volumetric radon activity in soil gas samples (Q, Bq/m^3), the CAMERA-01 complex with the sensitivity of 0.27 ± 0.03 Bq^{-1}s^{-1} and maximum permissible relative error of ±30% was used. According to the technique, the Q value obtained for the analyzed soil gas adsorbed in coal at the depth of 10–15 cm represented an integral (for two days) and absolute estimate of volumetric radon activity at the sample point. Measurement points formed cross-line profiles for the studied faults. Most profiles had similar intervals between measurement points with detailing at the intersection with the fault plane clearly indicated by a tectonic scarp (Fig. 1*B*), as well as a trench or a bar in seismic dislocation studies (Fig. 2*B*, *C*). Each fault

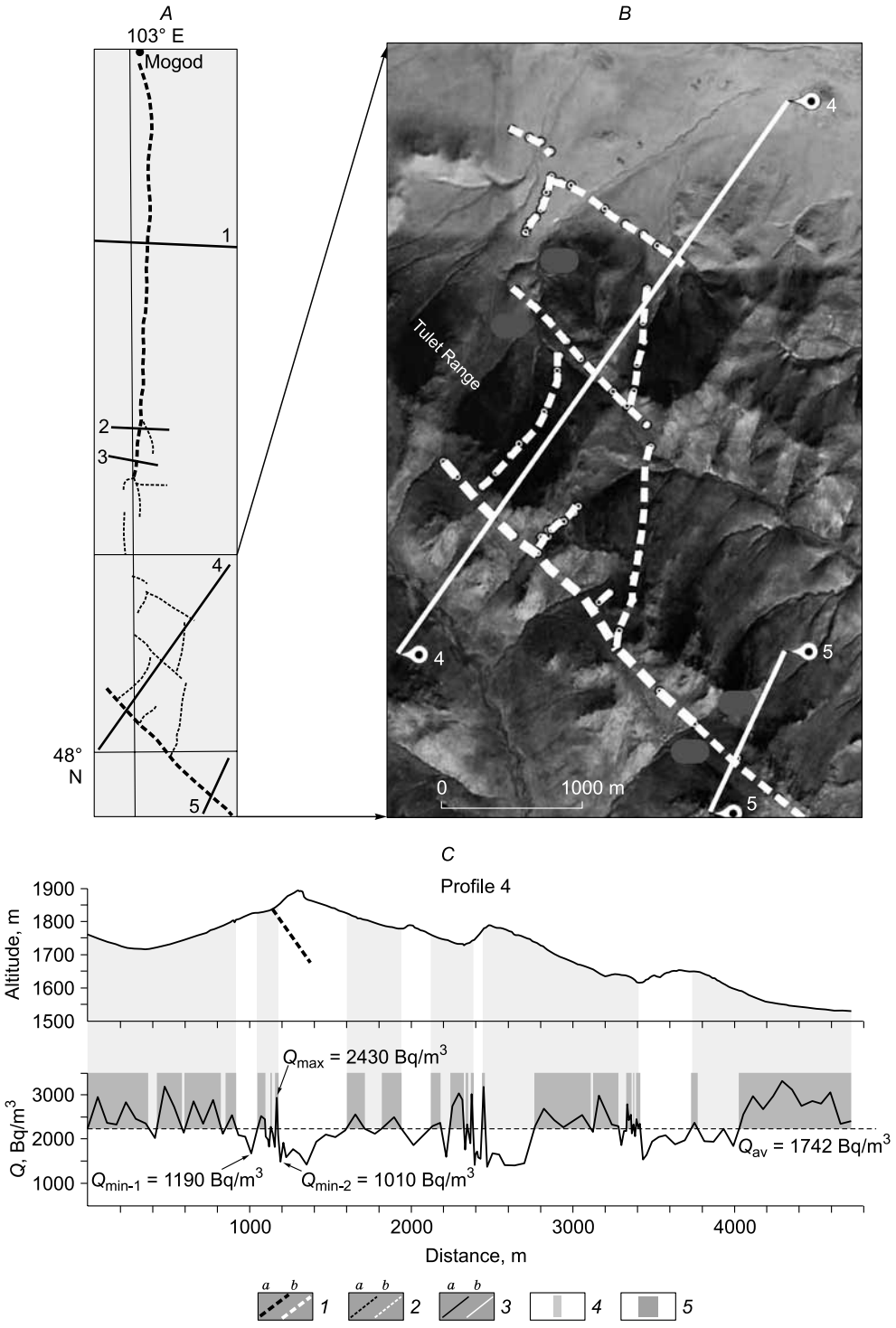

Fig. 2. Locations of emanation survey profiles in the Mogod area (*A*, *B*) and survey results for an individual profile (*C*). *A*, locations of emanation survey profiles intersecting the seismic rupture network formed in 1967 following the strong Mogod earthquake (M = 7.8); *B*, locations of two emanation survey profiles intersecting the thrust branch of the seismic rupture in the satellite image; *C*, variations in absolute topographic markers (top) and volumetric soil radon activity Q (bottom) along the profile 4 intersecting the primary and secondary reverse fault seismic ruptures. *1*, primary seismic ruptures in *A* and *C* (*a*) and B (*b*); *2*, secondary seismic ruptures in *A* (*a*) and *B* (*b*); *3*, emanation survey profiles (with numbers) in *A* (*a*) and *B* (*b*); *4*, near-fault radon anomalies; *5*, profile segments with anomalous soil radon concentrations ($Q > Q_{avg}$). Q_{max}, Q_{min-1}, and Q_{min-2} — radon anomaly parameters used for calculating K_Q for the primary reverse fault seismic rupture.

plane was usually studied using one or two profiles, however, it could be up to four profiles for fault zones with a complex structure (Table 1). Measurements within individual profiles were taken in the course of 1–2 days and within individual faults in the course of 2–10 days. The works were performed in dry summer and/or autumn seasons of 2010–2016, which made it possible to duplicate individual measurements within certain profile segments to study variations of Q in time.

It was shown by (Seminsky and Demberel, 2013) that variations in the Q values within individual profiles could be above an order of magnitude even with similar uranium contents in rocks disturbed by faults. Despite this, relative radon activity (K_Q) was used to reduce the role of nontectonic factors of emanation field formation, when comparing the ruptures from different geological and landscape-climatic settings. This parameter represented the relation of the intensity of the near-fault anomaly (Q_{max}) to the minimum Q value right beyond it ($Q_{min} = (Q_{min\text{-}1} + Q_{min\text{-}2})/2$) (Figs. 1*B*, 2*C*). K_Q values are less dependent on meteorological conditions and rock radioactivity than the absolute Q_{max} values. This contrast of a radon anomaly is primarily defined by the fault zone structure and its tectonic activity. K_Q makes it possible to identify ruptures with ultrahigh ($K_Q > 10$), high ($10 \geq K_Q > 5$), increased ($5 \geq K_Q > 3$), medium ($3 \geq K_Q > 2$), and low ($K_Q \leq 2$) radon activity.

In addition to contrast (K_Q) and intensity (Q_{max}), width (H) was determined for each near-fault anomaly. Here $Q > Q_{avg}$, where Q_{avg} is the arithmetic mean of all values measured within the profile (Figs. 1*B*, 2*C*), were considered anomalous. In most cases, near-fault anomalies appeared interrupted, since near-fault areas often included segments with low gas permeability (clay gouge and narrow massive blocks). Small segments of a profile with $Q < Q_{avg}$ were considered within the boundaries of the anomaly if they were located between two anomalous domains and were smaller than at least one of them.

RESEARCH RESULTS

The analysis of the emanation survey results is based on studying 20 profiles, whose lengths, as opposed to previous studies (Seminsky and Demberel, 2013), were selected to ensure full intersection of the near-fault anomaly. Quantitative parameters of radon anomalies identified within each profile are presented in Table 1, along with averaged parameters for faults based on 2–4 intersections. These estimates are highlighted in bold in Table 1 for the basis for the analysis performed.

Widths of near-fault radon anomalies in the vicinity of ruptures of various ranks vary from 80 to 1625 m (Table 1). Average values Q_{avg} for individual faults range from 1697 to 3516 Bq/m^3, intensity of near-fault anomalies Q_{max} from 2525 to 9298 Bq/m^3, and minimum values Q_{min} beyond their boundaries from 860 to 2990 Bq/m^3. K_Q values vary from 1.9 to 7.6, which makes it possible to divide the studied faults into four groups with high (Hustai-2, Skai), increased (Hustai-3, Sharai, Avdar, Gunjiin), medium (Emeelt, Mogod, Tulet), and low (Hustai-1) radon activity. The averaged estimates mentioned above remain valid and appropriately reflect emanation activity of disjunctive structures. However, the radon field is so unstable in terms of fault strikes that radon activity estimates for individual profiles may vary from medium to increased (Hustai-3, Emeelt) and ultrahigh (Hustai-2).

Dynamic formation conditions of faults have a significant effect on their radon activity, which increases in the following succession: compression–compression with shear–shear–extension with shear (Fig. 3*A*). This regularity observed for individual profiles (diamonds) and especially clearly for the whole faults (circles) is explained by the fact that strong extensional activity causes wider pore and fracture opening, which in turn increases gas migration towards the surface (Kemski et al., 1996; Richon et al., 2010; Utkin and Yurkov, 2010).

Fault rank also has a significant effect on the sizes of respective radon anomalies. H values vary rather widely among the faults of the same rank. However, the average values calculated based on the data from Table 1, are doubled mirroring fault lengths and reach 431 m for first-rank disjunctive structures and 825 m for second-rank faults. When the rank of the disjunctive structure and therefore the width of the near-fault radon anomaly increases, its contrast, according to average values, is maintained at the same level (K_Q = 3.8–3.9). Moreover, the sample generated based on strike-slip faults, which suppresses the effect of dynamic formation conditions of disjunctive structures, displays not only reduced K_Q (4.4 for rank 1; 3 for rank 2), but lower intensity of anomalies Q_{max} as well (5080 Bq/m^{3}for rank 1; 4251 Bq/m^3 for rank 2). The revealed regularity cannot be considered a coincidence, as it is confirmed by comparisons of K_Q and H of anomalies identified for the same fault within different profiles. It can be seen from Table 1 that radon activity decreases in most cases when the anomaly's width increases. It will be shown in the next section that low radon activity of second-rank faults compared to first-rank faults is due to differences in internal structures of research targets selected.

The effect of fault ranks and dynamic formation conditions on radon activity considered above reflects a significant role of endogenous deformation forces in emanation field formation, however, the direct effect of tectonic activity is primarily represented by movement intensity. Given the lack of reliable data on fault movement velocities for Central Mongolia, this parameter was estimated indirectly based on spatial-temporal seismicity manifestations in the study areas and in the immediate vicinity of research targets.

The spatial relationship between near-fault radon anomalies and seismic activity manifestations is shown by the fact that emanation anomaly parameters are higher for seismic active segments of the same fault than for aseismic seg-

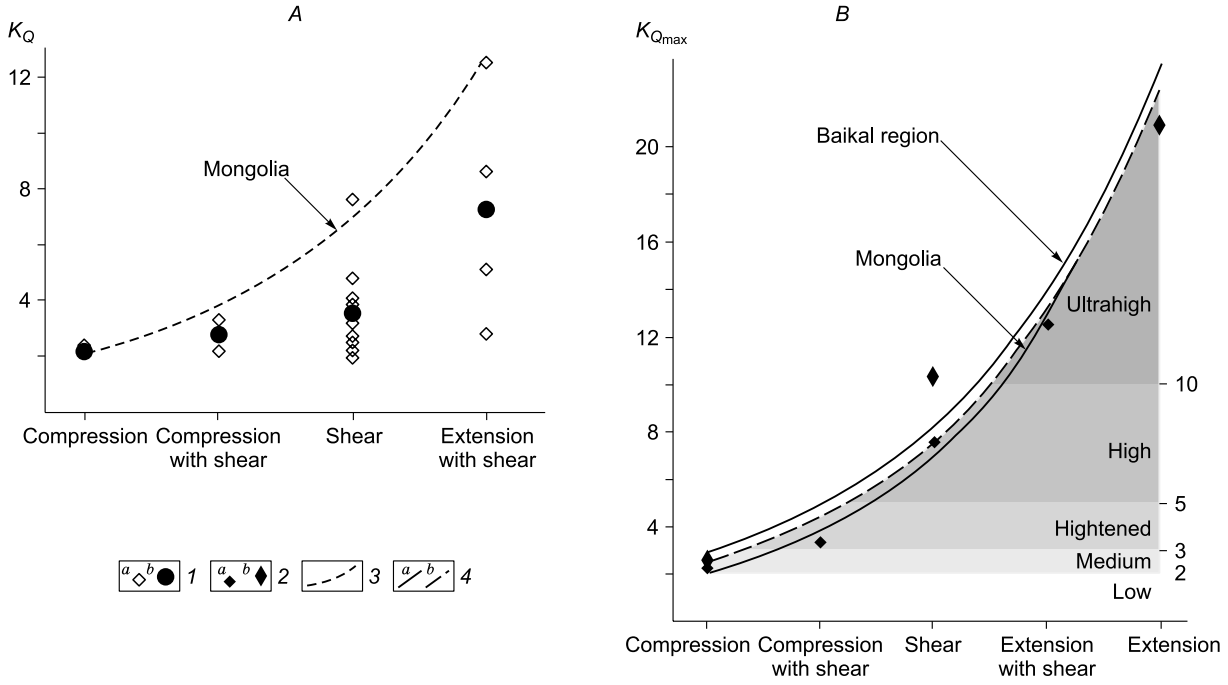

Fig. 3. Diagrams illustrating the effect of dynamic formation conditions of faults on their radon activity. *A*, diagram illustrating the effect of dynamic formation conditions of faults in Mongolia on their radon activity (K_Q); *B*, diagram illustrating the effect of dynamic formation conditions of faults in Mongolia and Baikal region on maximum radon activity values ($K_{Q\,\max}$) identified for each group of tectonic faults. *1*, symbols reflecting radon anomaly contrast (K_Q) in *A* for individual profiles (*a*) and on average for faults forming under all the studied dynamic settings (*b*); *2*, symbols reflecting maximum radon activity values ($K_{Q\,\max}$) in *B* calculated as averages for faults in Mongolia (*a*) and Baikal region (*b*) under all the studied dynamic settings; *3*, line reflecting the first approximation of the effect of dynamic formation conditions of faults on maximum radon activity values ($K_{Q\,\max}$); *4*, lines reflecting the first approximation of the effect of dynamic formation conditions of faults on averaged maximum radon activity values ($K_{Q\,\max}$) obtained for Mongolia and Baikal region separately (*a*) and combined (*b*). Gray scale represents radon activity levels of faults according to the accepted classification.

ments. This regularity was discussed in detail for the case of Hustai fault in the dedicated paper (Seminsky et al., 2014). At the same time, Skai fault, which is also located in the Ulaanbaatar area, is characterized by high radon activity in the absence of seismicity during the emanation survey (Table 1, Fig. 1*A*). We may assume that intense radon release, in this case, is linked to the high activity of this minor fault affected by endogenous or exogenous processes in the form of creep throughout the small, but well-formed surface of the main fault plane.

The temporal relationship between emanations and seismic activity is primarily reflected by the comparison of the number of earthquakes that occurred in Ulaanbaatar area (160 × 220 km) in various years and radon activity of the studied faults in respective years. Average K_Q and $Q_{\max}$ values calculated using the data from Table 1 remain approximately the same throughout the whole emanation survey except for 2013, when the analyzed values nearly doubled. The same pattern, but with the value tripled, was observed for the number of earthquakes (Fig. 4*A*). A similar trend was observed earlier for individual anomalies as well (Seminsky and Demberel, 2013). For instance (Fig. 4*B*), a decrease in intensity of the anomaly in the Emeelt fault area in 2011 to a third of its value in 2010 reflects a similar reduction in the number of earthquakes (201 events in 2010 and 542 in 2011).

The relation between the fault's seismic mode and its radon activity behavior is investigated for the seismic rupture formed as a result of the Mogod earthquake (M = 7.8; Jan 05, 1967). It can be seen from the profile intersecting the main thrust fault plane of the Tulet branch (Fig. 2*B*) that it is associated with the smallest of the identified anomalies. It demonstrates medium radon activity, similar to the Mogod strike-slip fault branch (Table 1). At the same time, larger and more intense anomalies are identified within the subdued topography in the profile, with the most intense and boundary anomalies not linked to secondary seismic ruptures (Fig. 2*A*). It is seemingly explained by the fact that the strong earthquake was followed by concentration of stresses, which now manifest themselves via activation of adjacent rupture structures clearly identified in the topography.

DISCUSSIONS

In this section we analyze whether the regularities concerning the effects of key parameters of faults, which reflect their tectonic activity directly or indirectly, on radon field identified using the example of Central Mongolia are common or local. It will make it possible to envision possible solutions for assessment of seismic hazards associated with

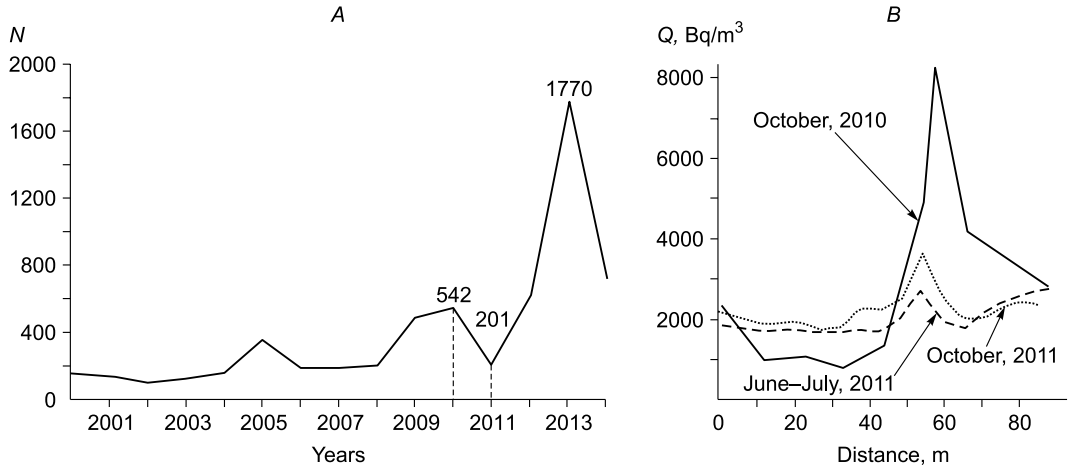

Fig. 4. Example of relation between seismic and radon activity in the Ulaanbaatar area. *A*, annual distribution of earthquakes with magnitudes M = 0.5–4.5 (N) in the Ulaanbaatar area in 2000–2014; *B*, temporal intensity variations for an individual soil radon anomaly (Q) associated with the Emeelt fault.

faults based on their emanation activity. First, the data of similar surveys performed in the Baikal region with the Earth's crust development driven by tectonic extension were used in the discussion (Seminsky and Bobrov, 2009). Second, the previous data were used, which, in one way or another, described relations between the intensities of near-fault emanations and morphogenesis of faults, their ranks, the state of internal structure, and intensity of movements reflected in seismicity or manifested in the form of creep for various regions of the world.

The effect of morphogenetic types of faults on their radon activity identified for Central Mongolia agrees with the generally accepted concept of more intense emanations corresponding to extensional tectonic settings compared to compressional settings. However, the opposite trend is also observed in some cases, for example, when compression and extension in the cross-line direction respectively lead to increased or decreased emanations, while strike-slip movements have no effect on radioactive gas concentrations, as illustrated by radon monitoring in cave air in the active fault area in Slovenia (Sebela et al., 2010).

These results seem to be the exceptions from the common trend associated with specific features of stress-deformed states of rocks and/or measurement conditions in specific settings. In general, considering the data from Baikal region (Seminsky and Bobrov, 2009), we may assume that radon activity of faults increases in dynamic settings (fault types) in the following succession: compression (reverse faults and overthrusts)–compression with shear (strike-slip reverse faults)–shear (dextral or sinistral strike-slip faults)–extension with shear (oblique-slip normal faults)–extension (normal faults). Furthermore, Fig. 3*A*, which clearly illustrates this trend in Mongolian faults, makes it possible to define an important peculiarity in the considered dependence. K_Q variation spectrum increases and probably in a nonlinear fashion with higher contribution of extension in the fault's formation conditions. It is evidenced by a dashed line that averages maximum values for all settings. A similar line plotted for Baikal region using the data from (Seminsky and Bobrov, 2009) (Fig. 3*B*) is slightly higher, which is reasonably explained by extensional crustal setting as opposed to strike-slip fault conditions in Central Mongolia, which are more constrained in terms of gas release.

Further dedicated research will make it possible to specify the locations of the considered curves for the Baikal region, Mongolia, and other regions by increasing the number of faults studied. At the current stage, we may use the averaged location of the curve (dashed line in Fig. 3*B*) to make essential conclusions for the problem being studied. For example, dynamic formation conditions of faults (or fault segments) limit the maximum values of radon activity. According to the presently available estimates, radon activity of faults in the studied areas may reach ultrahigh levels only when their formation conditions include a tectonic extension, i.e., in faults or oblique-slip faults (with various angles). Radon activity in ruptures of other morphogenetic types is usually limited to the following levels: high for strike-slip faults (dextral or sinistral); increased for strike-slip reverse faults (with various angles); medium for reverse faults (overthrusts). This classification provides additional opportunities for radon surveys in the considered landscape-climatic conditions: in addition to revealing faults hidden by loose drift, preliminary estimates of their formation conditions in the survey areas may be obtained.

The effect of the fault's size rank on its radon activity is represented by more intense radioactive gas release in areas of major disjunctive structures compared to smaller faults, according to the data from the Baikal region (Seminsky and Bobrov, 2009). However, in Mongolian targets increase in fault length is only accompanied by an increase in width of the radon anomaly, whereas radon activity shows no significant changes. It contradicts to a degree with the common

concept of lower tectonic (and seemingly radon) activity of smaller faults compared to major ones due to potential capability of the latter for higher-amplitude movements.

At the present stage, the results obtained for Mongolian targets may be attributed to differences in internal structures of crustal fault zones. According to tectonophysical data (Ben-Zion and Sammis, 2003; Seminsky, 2003, 2014), in extreme cases they may be represented by wide zones of multiple small ruptures (early-stage faulting) or narrow tectonite bands of the main fault plane, which is accompanied by secondary ruptures in some segments thereby forming echelon faults (late-stage faulting) (Fig. 5). Experimental investigations of fault movement amplitude distribution in the strike-slip fault formation area (San'kov and Seminsky, 1988) showed that a substantial part of amplitude in wide dispersed first-type faults (Fig. 5*A*, 2–4) is manifested in the form of plastic deformation and in second-type faults (Fig. 5*B*, 2–4) in the form of fault movements primarily in the main fault plane. Thus, concentrated late-stage faults are expected to have higher intensity and contrast of radon anomalies, other things being equal (see, for instance, Skai fault in the Ulaanbaatar area).

Thus, we do not have strong reasons to reassess conclusions about the direct link between radon activity of faults and their size rank at this research stage. Lower radon activity in Mongolian second-rank faults compared to first-rank

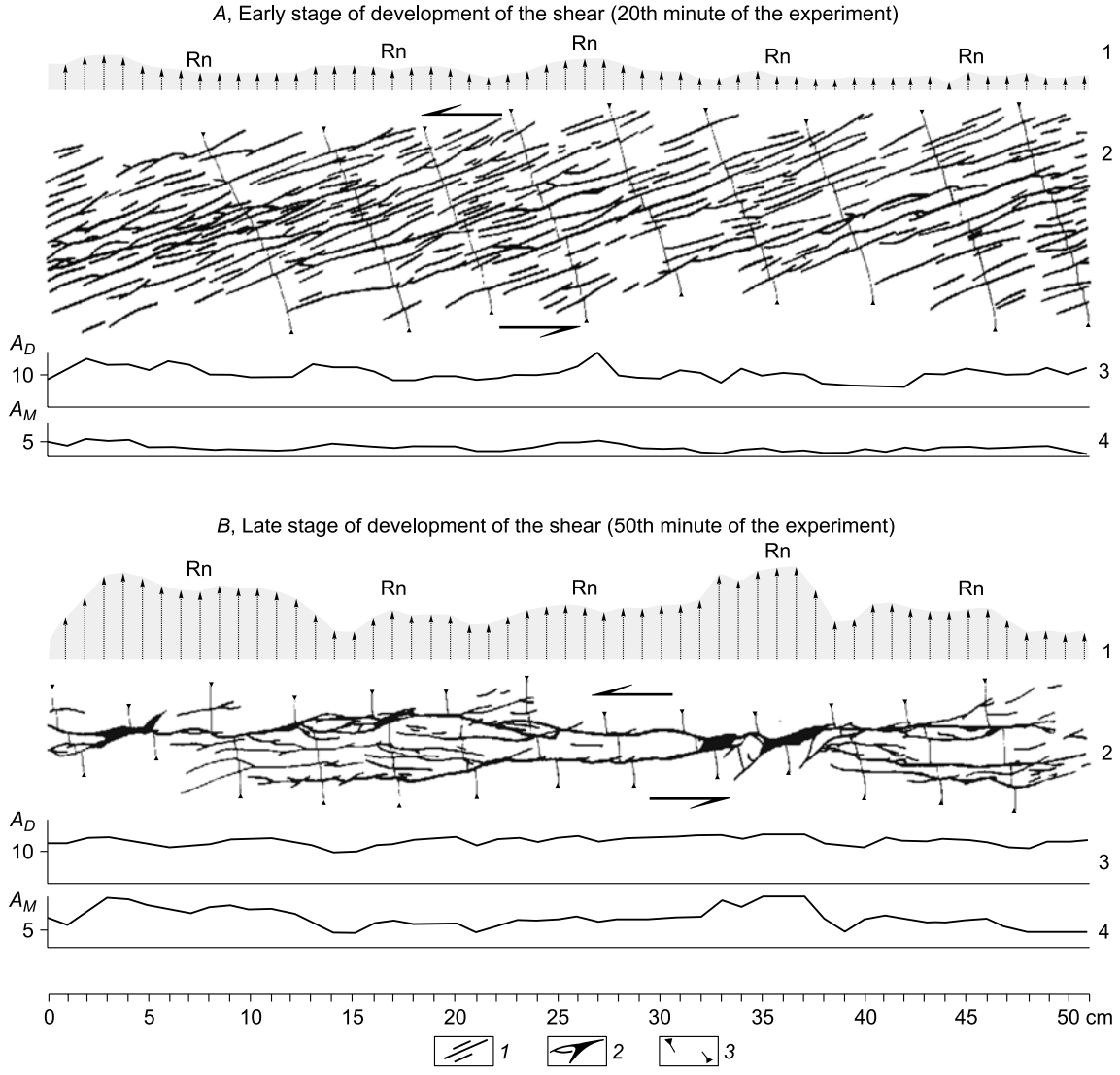

Fig. 5. Nonuniformity of a gas emanation field due to fault zone structure peculiarities at early (*A*) and late (*B*) development stages modeled using the example of a sinistral strike-slip fault forming under nearly ideal conditions of a laboratory experiment. *1*, strike-slip faults; *2*, ruptures with expansion component; *3*, markers in the form of rectilinear segments transverse to the strike of the fault zone placed at the surface of the model before deformation. 1, radon emanation variations along the fault zone (arrow lengths are proportional to the maximum movement amplitudes along one of the ruptures in the measurement area); 2, structures of active faults at the respective development stages of the strike-slip fault zone in the experiment with an elastoplastic material (wet clay); 3–4, variations in disjunctive component of total movement along the strike of the strike-slip fault zone (A_D, mm) (3) and maximum movement amplitude along one of the ruptures (A_M, mm) (4) in the measurement area plotted for two typical faulting stages (20 and 50 minutes of the experiment).

faults may be explained by differences in internal structures of the research targets selected. Smaller faults (Skai, Hustai-1, Gunjiin, etc.) are represented at the present development stage by main fault planes characterized by relatively intense emanations, whereas larger disjunctive structures (Hustai-2, Sharai, Avdar, etc.) are represented by wide rupture zones with radon anomalies with lower contrast. In general, it is confirmed by either absence of seismic activity (creep) or its concentration in the immediate vicinity of the fault plane in the first case or scattering of earthquake epicenters in the second case (Fig. 1*A*).

The effect of internal fault structure on their radon activity is therefore represented by a higher contrast of emanation anomalies associated with concentrated faults at late development stages compared to fault zones with dispersed structures at early development stages. In addition, differences in structure are the main cause of significant K_Q variations along fault strikes. It may be clearly illustrated by the example of the strike-slip zone, which develops in accordance with the elastoplastic model under nearly ideal conditions of a laboratory experiment (Fig. 5), which according to similarity theory match the generalized setting of major crustal faulting (Sherman et al., 1991). Despite the fact that deformation of a uniform clayey paste layer occurred at a constant rate in the absence of gravitational faulting and general shear amplitude remained the same along the strike of the rupture zone, its internal structure at each development stage was characterized by a greater or lesser degree of structural nonuniformity (Sherman et al., 1991; Seminsky, 2003).

It is manifested especially clearly at the late stage (Fig. 5*B*, 2), at which a clear-cut structural differentiation of the strike-slip zone in the in-line direction was defined based on numerous experimental data. Alteration of relatively thin segments of the future main fault plane, which demonstrate the full block movement amplitude (intervals 3–6, 32–37 cm), and wide junction areas between these segments, where general amplitude is defined by fault movements and a minor plastic component. This structural nonuniformity leads to significant differences in shapes of radon anomalies within cross-sections of the same disjunctive structure in profile surveys (King et al., 1993; Atallah et al., 2001; Zhou et al., 2010; Seminsky and Demberel, 2013), or alteration of maximum and minimum soil radon concentrations along fault zones in areal surveys (Ciotoli et al., 1999; Ball et al., 1991; Tansi et al., 2005; Ciotoli et al., 2007; Lombardi and Voltattorni, 2010; Walia et al., 2010). Apparently, radon activity of disjunctive structures varies in the in-line direction in this case, and the data of the present research show that these variations are explained by tectonic behavior.

Relation between seismic and radon activities of faults is a specific case of dependence of radon emanations on seismic mode in the area, which is fundamental for identification of emanation precursors of strong earthquakes. It was qualitatively demonstrated in Central Mongolia within the studies of spatial and temporal aspects. High radon emanation intensity in the Ulaanbaatar area corresponds to the higher number of earthquakes, the same being true for more seismic active fault segments as opposed to passive ones; low radon activity of faults following the strong seismic event is observed in the Mogod area, which increases in the adjacent rupture network elements. Close link between seismic and radon activities reflecting their dependence on stress-deformed state of rocks in the fault zone was described in other regions as well (Tansi et al., 2005; Lombardi and Voltattorni, 2010; Utkin and Yurkov, 2010; Koike et al., 2014; Papastefanou, 2010; Cigolini et al., 2015; Li et al., 2016; Zhou et al., 2017).

Relation between creep component of fault movement and radon activity was not estimated for disjunctive structures in Central Mongolia due to lack of the required data. Moreover, detailed studies of the relation between emanation intensity and movement velocities of fault sides are extremely rare in the literature on radon research. At the same time, emanation method of fault identification used intensely in many regions around the world is based on increase in radon release through tectonic fault zones as a result of crushing processes and higher substrate permeability due to displacement of fault sides. Some authors present data showing that radon emanations are directly linked with the dynamics of fault structures and deformation behavior of rock masses within them (Utkin and Yurkov 2010; Dalatkazin et al., 2013). Examples of more intense radon exhalation through aseismic fault segments compared to seismically active segments are available as well (Künze et al., 2012). Furthermore, increased soil radon concentrations are common in flanks of present-day landslides, where the most active rock mass movements (creep) occur (Sultankhodzhaev et al., 1979; Purtscheller et al., 1995; Wang, 2011).

Therefore, we may assume that the creep component of fault movement directly affects the gas emanation intensity. However, this statement, similarly to the conclusion regarding seismic activity, is only valid as a general regularity. Under specific emanation survey conditions, this pattern may manifest itself in different ways and may be difficult to identify. For instance, a series of publications is available, which describes the results of targeted research showing ambiguous relation between radon emanations and faults (Richon et al., 2010; Vaupotic et al., 2010; Mojze et al., 2017).

It seems that many cases of faults being poorly manifested in emanation fields may be successfully explained by complex structure of fault zones. For example, radon survey profile may provide only a partial coverage of a wide rupture zone or pass through a segment, where massive blocks with low gas permeability and/or fault planes filled with dense clay gouge prevail (Ball et al., 1991; King et al., 1993; Seminsky and Demberel, 2013). These situations, as well as structural settings of fault zones that facilitate intense radon exhalation, are presented in Fig. 5, which generalizes the experimental results regarding the formation of a major strike-slip fault under stable deformation mode.

Concepts of near-fault radon anomaly structure based on the analysis performed are presented in Fig. 5*A*, 1 and

5*B*, 1. Radon fluxes are indicated by arrows of different sizes above the diagrams of incipient and mature faults. They are defined by movement velocities proportional to fault movement amplitudes in the measurement areas, which may be represented by disjunctive component of the total movement amplitude (A_D) or movement amplitudes along the largest fault plane (A_M), which display similar variations along the faulting zone. Here, A_M was used for plotting an in-line profile of a hypothetic anomaly, since it is expected to be associated with the same rupture as Q_{max} in a profile radon survey.

Thus, Figs. 5*A*, 1 and 5*B*, 1 represent the basic model of a soil radon anomaly above the fault, whose structure is directly linked to fault activity represented by movement amplitude distribution, which in turn is defined by spatial-temporal regularities of faulting. Generally, dispersed faults at early development stages (Fig. 5*A*, 1) have higher anomaly intensities compared to concentrated disjunctive structures at late formation stages (Fig. 5*B*, 1). Despite stable deformation conditions, emanation anomaly structures are nonuniform in both settings. Radon anomalies are expected to have higher contrast and high K_Q within profiles intersecting the segments of the main fault plane with maximum movement amplitudes compared to wide areas of intense rupturing represented by relatively small faults, where total movement amplitudes are partially manifested in plastic deformations.

CONCLUSIONS

Emanation survey results for Central Mongolia show that faults and their key parameters, such as size rank, internal structure peculiarities, dynamic formation conditions, and seismic activity, have a significant effect on radon activity. Additional analysis of the radon survey data from other regions confirms the discovered regularities.

1. Emanation activity of faults in geodynamically active areas is an integral indicator of their tectonic behavior. If we consider movement intensity, which is a component of tectonic activity of great practical utility, then we can see that linking it directly to intensity or contrast of near-fault radon anomalies is complicated by morphogenesis and internal structure peculiarities of faults.

2. Radon activity of faults decreases with higher contribution of extension in faulting conditions, and in faults with internal structures insufficiently developed for intense emanation. In other words, other things being equal, higher K_Q are more common for faults and strike-slip faults compared to reverse faults (overthrusts) and for concentrated faults at late development stages compared to wide rupture zones at early stages of internal structure formation.

3. The nonuniform structure is an integral property of near-fault radon anomalies, which is still present even when faults develop under stable conditions, i.e., material uniformity of the deformed substrate and constant deformation rate. Spatial variations in radon activity are defined by variations in disjunctive component of the movement amplitude and the degree of rupturing in the fault zone. The well-known alteration of maximum and minimum soil radon concentrations along the fault, as well as a nonuniform decrease in emanation intensity from the periphery of the fault zone towards its axial part, are primarily explained by specific changes in the internal structure.

The discovered regularities make it possible to envision possible ways of estimating the effect of the considered tectonic activity parameters on near-fault emanation parameters, which could facilitate a more accurate assessment of hazards associated with faults based on radon survey data.

The authors thank S.A. Bornyakov, Yu.P. Burzunova, and A.K. Seminsky of the Institute of the Earth's Crust of the Siberian Branch of the Russian Academy of Sciences and D. Ganzorig, D. Mungusuren, and M. Bilguun of the Institute of Astronomy and Geophysics of the Mongolian Academy of Sciences for participation in radon survey and processing of the results. The work was supported in part by the Russian Foundation for Basic Research (project No. 16-55-44017).

REFERENCES

Atallah, M.Y., Al'Bataina, B.A., Mustafa, H., 2001. Radon emanation along the Dead Sea transform (rift) in Jordan. Environ. Geol. 40, 1440–1446.

Ball, T.K., Cameron, D.G., Colman, T.B., Roberts, P.D., 1991. Behaviour of radon in the geological environment: a review. Q. J. Eng. Geol. 24, 169–182.

Bano, M., Tsend-Ayush, N., Schlupp, A., Munkhuu, U., Davaasambuu, B., Enkheee, B., Battsetseg, B., 2017. Studying active faults by GPR technique: example of Songino fault, Ulaanbaatar, in: Proc. Int. Conf. on Astr. Geophys. in Mongolia, 2017. Ulaanbaatar: Mongol Altay Printing Co. ltd., pp. 137–142.

Bayasgalan, A., Jackson, J., 1999. A re-assessment of the faulting in the 1967 Mogod earthquakes in Mongolia. Geophys. J. Int. 138, 784–800.

Ben-Zion, Y., Sammis, C.G., 2003. Characterization of fault zones. Pure Appl. Geophys. 160, 677–715.

Cigolini, C., Laiolo, M., Coppola, D., 2015. The LVD signals during the early-mid stages of the L'Aquila seismic sequence and the radon signature of some aftershocks of moderate magnitude. J. Environ. Radioactiv. 139, 56–65.

Ciotoli, G., Etiope, G., Guerra, M., Lombardi, S., 1999. The detection of concealed faults in the Ofanto Basin using the correlation between soil gas fracture surveys. Tectonophysics 301, 321–332.

Ciotoli, G., Lombardi, S., Annunziatellis, A., 2007. Geostatistical analysis of soil gas data in a high seismic intermontane basin: Fucino Plain, central Italy. J. Geoph. Res. 112, B05407.

Dalatkazin, T.Sh., Konovalova, Yu.P., Rouchkin, V.I., 2013. Experimental researches of using radon concentration measurements for district's geodynamic dividing. Litosfera, No. 3, 146–150.

Kemski, J., Klingel, R., Siehl, A., 1996. Classification and mapping of radon affected areas in Germany. Environ. Int. 22, S789–S798.

King, C.-Y., Zhang, W., King, B.-S., 1993. Radon anomalies on three kinds of faults in California. Pure Appl. Geophys. 141 (1), 111–124.

Koike, K., Yoshinaga, T., Ueyama, T., Asaue, H., 2014. Increased radon-222 in soil gas because of cumulative seismicity at active faults. Earth Planet. Space 66: 57. DOI: 10.1186/1880-5981-66-57.

Künze N., Koroleva M., Reuther C.-D., 2012. ^{222}Rn activity in soil gas across selected fault segments in the Cantabrian Mountains, NW Spain. Radiat. Meas. 47, 389–399.

Li, C., Su, H., Zhang, H., Zhou, H., 2016. Correlation between the spatial distribution of radon anomalies and fault activity in the northern margin of West Qinling Fault Zone, Central China. J. Radioanal. Nucl. Chem. 308, 679–686.

Lombardi, S., Voltattorni, N., 2010. Rn, He and CO2 soil gas geochemistry for the study of active and inactive faults. Appl. Geochem. 25, 1206–1220.

Mojze, A., Marko, F., Porubcanova, D., Bartosova, A., 2017. Radon measurements in an area of tectonic zone: a case study. J. Environ. Radioactiv. 166, 278–288.

Papastefanou, C., 2010. Variation of radon flux along active fault zones in association with earthquake occurrence. Rad. Measur. 45, 943–951.

Purtscheller, F., Pirchi, T., Sieder, G., Stingl, V., Tessadri, N., Brunner, P., Ennemoser, O., Schneider, P., 1995. Radon emanation from giant landslides of Koefels (Tyrol, Austria) and Langtang Himal (Nepal). Environ. Geol. 26, 32–38.

Richon, P., Klinger, Y., Tapponnier, P., Li C., Woerd, J.V.D., Perrier, F., 2010. Measuring radon flux across active faults: Relevance of excavating and possibility of satellite discharges. Radiat. Meas. 45, 211–218.

San'kov, V.A., Seminsky, K.Zh., 1988. Analysis of fault movements in a developing transform fault area. Izvestiya VUZov. Geologiya i Razvedka, No. 4, 10–18.

Sebela, S., Vaupotic, J., Kostak, B., Stemberk, J., 2010. Direct measurement of present-day tectonic movement and associated radon flux in Postojna Cave, Slovenia. J. Cave Karst Stud. 72 (1), 21–34.

Seminsky, K.Zh., 2003. Internal Structure of Continental Fault Zones. The Tectonophysical Aspect [in Russian]. Akad. Izd. Geo, Novosibirsk.

Seminsky, K.Zh., 2014. Specialized mapping of crustal fault zones. Pt. 1: Basic theoretical concepts and principles. Geodyn. Tectonophys. 5 (2), 445–467.

Seminsky, K.Zh., Bobrov, A.A., 2009. Radon activity of faults (western Baikal and southern Angara areas). Russian Geology and Geophysics (Geologiya i Geofizika) 50 (8), 682–692 (881–896).

Seminsky, K.Zh., Demberel, S., 2013. The first estimations of soil-radon activity near faults in Central Mongolia. Radiat. Meas. 49, 19–34.

Seminsky, K.Zh., Bobrov, A.A., Demberel, S., Burzunova, Yu.P., Mungunsuren, D., Oyun-Erdene, M., Seminsky, A.K., Bilguun, M., Tarasova, A.A., 2014. Hustai fault area (Central Mongolia): Emanation survey results. Izvestiya SO SNZ RAEN, No. 6 (49), 68–81.

Seminsky, K.Zh., Demberel, S., Mungunsuren, D., 2017. Fault zones and stress fields of the Earth's crust in the vicinity of Ulaanbaatar (Mongolia) at the modern stage of tectogenesis. Dokl. Earth Sci. 474 (1), 511–515.

Sherman, S.I., Seminsky, K.Zh., Bornyakov, S.A., 1991. Faulting in the Lithosphere. Shear Zones [in Russian]. Nauka, Novosibirsk.

Sultankhodzhaev, A.N., Tyminskii, V.G., Spiridonov, A.I., 1979. Radioactive Emanations in Studies of Geological Processes [in Russian]. Fan UzSSR, Tashkent.

Tansi, C., Tallarico, A., Iovine, G., Gallo, M.F., Falcone, G., 2005. Interpretation of radon anomalies in seismotectonic and tectonic-gravitational settings: the south-eastern Crati graben (Northern Calabria, Italy). Tectonophysics 396, 181–193.

Toutain, J.-P., Baubron, J.-C., 1999. Gas geochemistry and seismotectonics: a review. Tectonophysics 304, 1–27.

Utkin, V.I., Yurkov, A.K., 2010. Radon as a tracer of tectonic movements. Russian Geology and Geophysics (Geologiya i Geofizika) 51 (2), 220–227 (277–286).

Vaupotic, J., Gregoric, A., Kobal, I., Zvab, P., Kozak, K., Mazur, J., Kochowska, E., Grzadziel, D., 2010. Radon concentration in soil gas and radon exhalation rate at the Ravne Fault in NW Slovenia. Nat. Hazards Earth Syst. Sci. 10, 895–899.

Walia, V., Lin, S.J., Fu, C.C., Yang, T.F., Hong, W.-L., Wen, K.-L., Chen, C.-H., 2010. Soil-gas monitoring: a tool for fault delineation studies along Hsinhua Fault (Tainan), Southern Taiwan. Appl. Geochem. 25, 602–607.

Wang, X.Q., 2011. Radon anomaly analysis of engineering slopes. Adv. Mater. Res. 261–263, 1161.

Zhou, H., Su, H., Zhang, H., Li, C., 2017. Correlations between soil gas and seismic activity in the Generalized Haiyuan Fault Zone, north-central China. Nat. Hazards 85, 763–776.

Zhou, X., Du, J., Chen, Z., Cheng, J., Tang, Y., Yang, L., Xie, C., Cui, Y., Liu, L., Yi, L., Yang, P., Li, Y., 2010. Geochemistry of soil gas in the seismic fault zone produced by the Wenchuan Ms 8.0 earthquake, southwestern China. Geochem. Trans. 11 (5), 1–10.

Editorial responsibility: A.D. Duchkov